# Detection of marine methane emissions with AVIRIS band ratios

Eliza S. Bradley,[1] Ira Leifer,[2] Dar A. Roberts,[1,3] Philip E. Dennison,[4] and Libe Washburn[1,3]

Received 31 January 2011; revised 2 April 2011; accepted 5 April 2011; published 20 May 2011.

[1] The relative source contributions of methane ($CH_4$) have high uncertainty, creating a need for local-scale characterization in concert with global satellite measurements. However, efforts towards methane plume imaging have yet to provide convincing results for concentrated sources. Although atmospheric $CH_4$ mapping did not motivate the Airborne Visible/Infrared Imaging Spectrometer (AVIRIS) design, recent studies suggest its potential for studying concentrated $CH_4$ sources such as the Coal Oil Point (COP) seep field (~0.015 Tg $CH_4$ $yr^{-1}$) offshore Santa Barbara, California. In this study, we developed a band ratio approach on high glint COP AVIRIS data and demonstrate the first successful local-scale remote sensing mapping of natural atmospheric $CH_4$ plumes. Plume origins closely matched surface and sonar-derived seepage distributions, with plume characteristics consistent with wind advection. Imaging spectrometer data may also be useful for high spatial-resolution characterization of concentrated, globally-significant $CH_4$ emissions from offshore platforms and cattle feedlots.
**Citation:** Bradley, E. S., I. Leifer, D. A. Roberts, P. E. Dennison, and L. Washburn (2011), Detection of marine methane emissions with AVIRIS band ratios, *Geophys. Res. Lett.*, *38*, L10702, doi:10.1029/2011GL046729.

## 1. Introduction

[2] Methane, $CH_4$, is an important greenhouse gas, with a global radiative forcing only second to carbon dioxide, $CO_2$, yet there are large uncertainties associated with the strength of different $CH_4$ sources, such as geological seeps [*Forster et al.*, 2007]. Imaging spectrometry has the potential for $CH_4$ mapping based on shortwave infrared (SWIR) radiance anomalies [*Frankenberg et al.*, 2005; *Gerilowski et al.*, 2010; *Schneising et al.*, 2009; *Yoshida et al.*, 2010], and at resolutions finer than 20 m can provide spatially-complete contextual information for integration with other datasets.

[3] The Airborne Visible/Infrared Imaging Spectrometer (AVIRIS), which measures radiance from 400–2500 nm at a nominal 10 nm resolution, has been used for earth system science since 1987 with a focus on geology and terrestrial ecology [*Green et al.*, 1998]. Greenhouse gas mapping with AVIRIS is nascent, but promising; a recent study identified marine seep $CH_4$ anomalies using a residual-based approach [*Roberts et al.*, 2010]. However, identification of $CH_4$ plume structure was confounded by oil slicks, meteorological conditions, radiance spectral features and lower/variable sun glint [*Roberts et al.*, 2010].

[4] An alternate remote sensing approach for $CH_4$ anomaly mapping is band ratio analysis, such as that used for fire detection [*Dennison and Roberts*, 2009], which has low computational demands and does not depend on atmospheric and surface parameterizations. Due to wavelength dependence of atmospheric gas absorption coefficients, negative anomalies in band ratio images can be indicative of increased gas absorption at the numerator wavelength or decreased gas absorption for the denominator. MODTRAN [*Berk et al.*, 1999] simulations illustrated $CH_4$ sensitivity for the reflectance ratio: 2325-nm ($CH_4$ absorbing) and 2125-nm (window) [*Larsen and Stamnes*, 2006]; however, to our knowledge this has yet to be replicated with actual sensor data. Our study addresses this limitation and explores additional band ratios for $CH_4$ detection using AVIRIS imagery of the Coal Oil Point (COP) marine hydrocarbon seep field.

[5] Marine geological hydrocarbon seeps are widespread, occur on all continental shelves and release considerable $CH_4$, on the order of ~20 Tg $yr^{-1}$ [*Kvenvolden and Rogers*, 2005]. This estimate is poorly constrained because of a lack of quantitative flux measurements and uncertainty in the fraction of seabed $CH_4$ that reaches the atmosphere [*Kvenvolden and Rogers*, 2005]. Arguably, the COP seep field (Figure S1 and Text S1 of the auxiliary material) is the best studied and among the most prolific seepage areas in the world [*Hornafius et al.*, 1999]. Total COP atmospheric emissions are estimated conservatively at 100,000 $m^3$ $day^{-1}$ (0.015 Tg $yr^{-1}$) based on sonar survey data and direct flux measurements [*Hornafius et al.*, 1999]. Seabed gas is primarily $CH_4$ (~80%) and $CO_2$ (~12%) [*Clark et al.*, 2010a]. Preferential bubble dissolution of lighter n-alkanes and air uptake decrease the bubble $CH_4$ fraction at the sea surface to 50–70% and $CO_2$ to trace levels (<0.1%) [*Clark et al.*, 2010a; *Leifer et al.*, 2006].

## 2. Data and Methodology

[6] AVIRIS data for the COP seep field were acquired on 19 June 2008 at 1200 LT (Local Standard Time, UTC-8) at 8.95 km altitude during clear sky conditions. Winds were from the southwest and light (2.3 m $s^{-1}$ from 236°) for 1130 – 1200 LT (West Campus Station, Figure S1a). Surface currents in the seep field were largely to the west–northwest and moderately strong (~25 cm $s^{-1}$, UCSB Surface Current Mapping Network) as part of an overall channel-scale counterclockwise circulation. The surface current data are

[1]Department of Geography, University of California, Santa Barbara, California, USA.
[2]Marine Science Institute, University of California, Santa Barbara, California, USA.
[3]Earth Research Institute, University of California, Santa Barbara, California, USA.
[4]Department of Geography and Center for Natural and Technological Hazards, University of Utah, Salt Lake City, Utah, USA.


0094-8276/11/2011GL046729

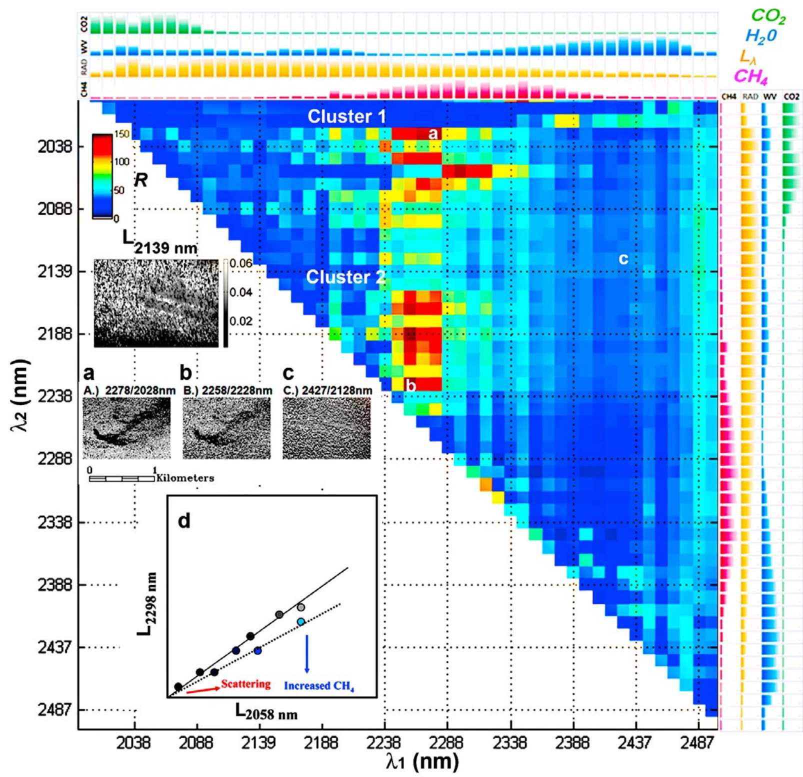


**Figure 1.** Normalized range values, $R$, from ratio image Trilogy Seep transects as a function of numerator wavelength ($\lambda_1$) and denominator ($\lambda_2$). Normalized scale bars of atmospheric absorption ($CO_2$, $H_2O$, and $CH_4$) and radiance are shown to the top and right. (a–c) Pixels labeled *a*, *b*, and *c* on the matrix refer to ratio images. (d) Schematic of radiance $L_{2298\ nm}$ versus $L_{2058\ nm}$, lighter colors represent higher albedo and points along the lower line are for increased $CH_4$.

averaged over circles 3 km in radius and are interpolated onto a 2 km square grid. Waves were from the southwest (243°) with a significant wave height of 1.0 m (NOAA NDBC buoy 46126). The COP seeps were sonar surveyed in 2005 [*Leifer et al.*, 2010] and Trilogy Seep was flux buoy surveyed on 19 and 20 September 2005 [*Clark et al.*, 2010a].

[7] AVIRIS radiance ratios for the Trilogy subset were calculated for the 51 bands in the SWIR-2 spectral region (2000 to 2500 nm) and secondary analysis (Text S2) was performed for the SWIR-1 (1400−1800 nm), which has weaker $CH_4$ absorption [*Roberts et al.*, 2010]. Anomaly strength associated with Trilogy Seep was assessed in terms of the normalized band ratio's amplitude ($R$) for seep transects (Figure S2) and corroborated by other methods (Figure S3). $R$ values were interpreted in terms of $CH_4$, $CO_2$, and water vapor sensitivity from MODTRAN simulations (Figures 1 and S4). The $L_{2298nm}/L_{2058nm}$ ratio image (Figure 2), $\zeta$, which had a high $R$ value and strong anomaly associated with Trilogy Seep, was detrended and mean filtered to produce $\zeta_f$ (Figure S5), which was fit with Gaussian models (Figure S6).

## 3. Results and Discussion

[8] High values of $R$ occurred in two clusters (Figure 1), both of which had $CH_4$-sensitive numerators ($\lambda_1$ ~2240 – 2340 nm). For the first cluster, $C_1$, the denominators were sensitive to $CO_2$ ($\lambda_2$ ~2030 – 2090 nm), while for $C_2$, weak $CH_4$ and water vapor ($\lambda_2$ ~2160 – 2230 nm). Combinations of $CH_4$ and $CO_2$ bands were effective for discriminating $CH_4$ anomalies and performed better than the residual-based approach for this scene (see Text S3) because radiances were similar for the pairs and unaffected by sensor saturation (Figure S7) and $CO_2$ is well-mixed in the scene compared to $CH_4$. Scaling by radiance from a $CO_2$-sensitive band corrects for multiplicative effects due to atmospheric pathlength and albedo. These results for AVIRIS agree with SCIAMACHY algorithms, where the vertical column density of $CH_4$ is normalized by $CO_2$, which has significantly less total column variability [*Frankenberg et al.*, 2005].

[9] The strongest band ratio $\zeta$ anomaly corresponded well with the sonar and flux buoy maps of Trilogy Seep (5000 $m^3$ gas $day^{-1}$) (Figure 2). Other seeps including Horseshoe (3000 $m^3$ gas $day^{-1}$) [*Clark et al.*, 2010a] and IV Super Seeps were also evident; however, for some weaker sonar sources (BPL and unnamed seep area "X", Figure 2b) there was no or only faint $\zeta$ expression. This could be attributable to AVIRIS sensitivity limitations, but also to seep emission variability (see Text S1), given that the sonar data were collected three years prior to the AVIRIS acquisition and weaker seeps can have lower persistence [*Bradley et al.*, 2010].

[10] The dispersive nature of the negative $\zeta$ anomalies (Figure 2b) following the wind direction as opposed to surface currents and discordance with dominant surface albedo variations (Figure S8) support an atmospheric, rather than surface, classification. Oil slick features generally are

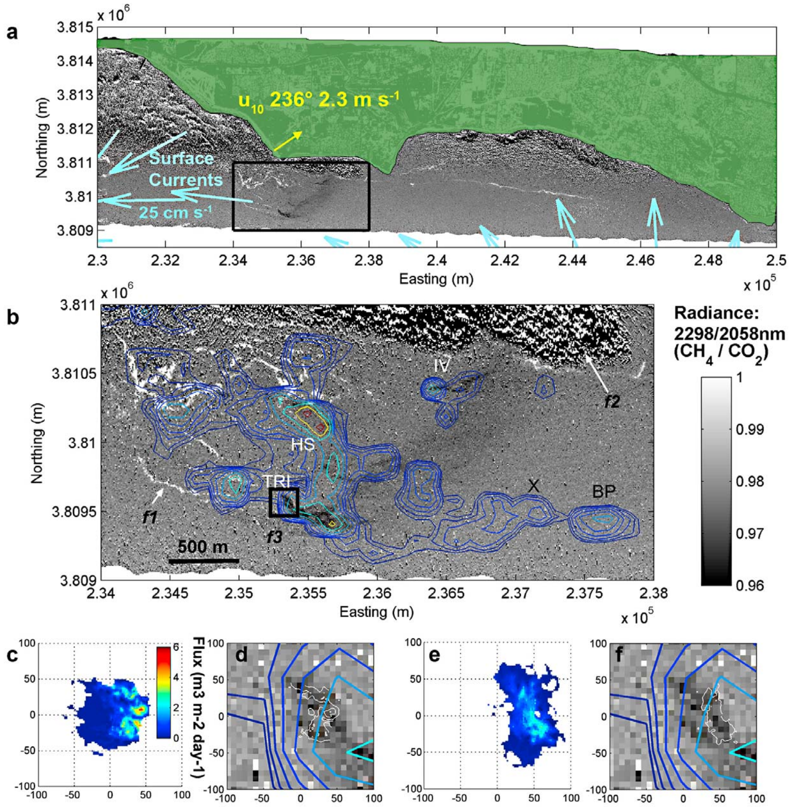


**Figure 2.** (a) AVIRIS $CH_4$ index, $\zeta$, ($L_{2298}/L_{2058}$) with wind vector at WCS and surface currents. (b) $\zeta$ subset overlain with sonar return contours (Figure S1). Labeled major seeps include IV Super Seep (IV), Horseshoe Seep (HS), and Trilogy Seep (TRI), while weak seeps include Bruce P Seep (BP) and unnamed "X" Seep (X). High $\zeta$ value features trending with currents (*f*1), noise dominates low radiance areas (*f*2) and potential outgassing (*f*3) down-current of TRI. (c) Trilogy seep gas flux from 19 September 2005 flux buoy measurements. Black square in Figure 2b indicates the 200 by 200 m subset location. (d) Superposition of $\zeta$, sonar, and gas flux contours (1:2:6 $m^3$ $m^{-2}$ $day^{-1}$). (e, f) Same as Figures 2c and 2d but for 20 September 2005. Flux data color bar in Figure 2c.

convergent due to processes such as Langmuir circulation [*Lehr and Simecek-Beatty*, 2000] and have distinct spectral features at shorter wavelengths [*Clark et al.*, 2010b]. Although the band ratio approach was relatively robust with regards to scene albedo (Figure S8), the effect of surface reflectance variability was not eliminated completely. Meandering positive $\zeta$ anomalies were identified that trended with ocean currents (Figure 2b, *f*1) and likely represented ocean surface features (e.g., oil-slicks, windrows), with a spectral bias between radiances at 2058 and 2298 nm, which also dominated the SWIR-1 band ratio analysis (Text S2 and Figures S8i and S8j). Furthermore, $\zeta$ plume identification was limited to regions with high sunglint; for lower radiance the signal-to-noise ratio decreased and the index $\zeta$ became unstable (north portion Figure 2a, plume northeast of IV Seep Figure 2b, *f*2).

[11] Application of the band ratio technique to other, less-optimal COP AVIRIS data, including the 6 August 2007 image in *Roberts et al.* [2010], produced positive methane anomalies in areas of known seepage, but not clearly identifiable plumes as was the case for the 19 June 2008 data, which had high sun glint, divergent wind and current vectors, and cloud-free conditions. Flight planning and timing is a critical component of successful AVIRIS $CH_4$ detection, although efforts are also being directed towards developing approaches suited for sub-optimal data analysis. Although the band-ratio based $CH_4$ index is a relative measure of $CH_4$ concentrations, the potential exists for calibration based on the residual-based technique or adaption of SCIAMACHY-developed methods [*Frankenberg et al.*, 2005; *Schneising et al.*, 2009], which would allow for flux estimations using a Gaussian plume model (see Text S4 for further discussion and complicating data issues).

[12] This study illustrates the utility of airborne imaging spectrometry for studying strong $CH_4$ sources, as demonstrated with AVIRIS data for the COP seep field. The $CH_4$ band ratio anomalies were consistent with seepage distribution and prevailing winds and provided insight into dynamics, e.g., (1) sharp seep-collocated anomalies were consistent with buoyantly rising plumes in agreement with interpretation of near-surface spectrometry and in situ measurements [*Leifer et al.*, 2006]) and (2) different modes of emission, such as evasion, may also be evident (*f*3 Figures 2b and S5). Imaging spectrometer data can provide the unique spatial characterization of strong $CH_4$ emissions that point measurements, linear transects, and coarse resolution data cannot. Imaging spectrometry also provides the necessary spectral and spatial information to study $CH_4$

sources within a spatial context, e.g., delineating landfill extent, mapping rice paddy water vapor gradients as was done for a poplar plantation [*Ogunjemiyo et al.*, 2002], and identifying offshore oil platforms.

[13] **Acknowledgments.** Research support was provided by the NASA North American Carbon Program (NNX07AC89G; Co-PI I.L. and D.R); UC Chancellor's fellowship; Bureau of Ocean Energy Management, Regulation, and Enforcement; and the CA State Lands Commission.

[14] The Editor thanks two anonymous reviewers for their assistance in evaluating this paper.

## References

Berk, A., et al. (1999), MODTRAN 4 radiative transfer modeling for atmospheric correction, paper presented at Optical Spectroscopic Techniques and Instrumentation for Atmospheric and Space Research III, SPIE, Denver, Colo.

Bradley, E., et al. (2010), Long-term monitoring of a marine geologic methane source by a coastal air pollution station in Southern California, *Atmos. Environ.*, *44*(38), 4973–4981, doi:10.1016/j.atmosenv.2010.08.010.

Clark, J., et al. (2010a), Variability of gas composition and flux intensity in natural marine hydrocarbon seeps, *Geo Mar. Lett.*, *30*(3–4), 379–388, doi:10.1007/s00367-009-0167-1.

Clark, R. N., et al. (2010b), A method for quantitative mapping of thick oil spills using imaging spectroscopy, *U.S. Geol. Surv. Open File Rep., 2010-1167*, 51 pp.

Dennison, P. E., and D. A. Roberts (2009), Daytime fire detection using airborne hyperspectral data, *Remote Sens. Environ.*, *113*(8), 1646–1657, doi:10.1016/j.rse.2009.03.010.

Forster, P., et al. (2007), Changes in atmospheric constituents and in radiative forcing, in *Climate Change 2007: The Physical Science Basis. Contribution of Working Group I to the Fourth Assessment Report of the Intergovernmental Panel on Climate Change*, edited by S. Solomon et al., pp. 129–234, Cambridge Univ. Press, Cambridge, U. K.

Frankenberg, C., et al. (2005), Assessing methane emissions from global space-borne observations, *Science*, *308*(5724), 1010–1014, doi:10.1126/science.1106644.

Gerilowski, K., et al. (2010), MAMAP - a new spectrometer system for column-averaged methane and carbon dioxide observations from aircraft: Instrument description and performance assessment, *Atmos. Meas. Tech. Discuss.*, *3*(4), 3199–3276, doi:10.5194/amtd-3-3199-2010.

Green, R. O., et al. (1998), Imaging spectroscopy and the Airborne Visible/Infrared Imaging Spectrometer (AVIRIS), *Remote Sens. Environ.*, *65*(3), 227–248, doi:10.1016/S0034-4257(98)00064-9.

Hornafius, J. S., D. Quigley, and B. P. Luyendyk (1999), The world's most spectacular marine hydrocarbon seeps (Coal Oil Point, Santa Barbara Channel, California): Quantification of emissions, *J. Geophys. Res.*, *104*(C9), 20,703–20,711, doi:10.1029/1999JC900148.

Kvenvolden, K. A., and B. W. Rogers (2005), Gaia's breath—Global methane exhalations, *Mar. Pet. Geol.*, *22*(4), 579–590, doi:10.1016/j.marpetgeo.2004.08.004.

Larsen, N. F., and K. Stamnes (2006), Methane detection from space: Use of sunglint, *Opt. Eng.*, *45*(1), 016202, doi:10.1117/1.2150835.

Lehr, W. J., and D. Simecek-Beatty (2000), The relation of Langmuir circulation processes to the standard oil spill spreading, dispersion, and transport algorithms, *Spill Sci. Technol. Bull.*, *6*(3–4), 247–253, doi:10.1016/S1353-2561(01)00043-3.

Leifer, I., et al. (2006), Natural marine seepage blowout: Contribution to atmospheric methane, *Global Biogeochem. Cycles*, *20*, GB3008, doi:10.1029/2005GB002668.

Leifer, I., et al. (2010), Geologic control of natural marine hydrocarbon seep emissions, Coal Oil Point seep field, California, *Geo Mar. Lett.*, *30*, 331–338, doi:10.1007/s00367-010-0188-9.

Ogunjemiyo, S., et al. (2002), Evaluating the relationship between AVIRIS water vapor and poplar plantation evapotranspiration, *J. Geophys. Res.*, *107*(D23), 4719, doi:10.1029/2001JD001194.

Roberts, D. A., et al. (2010), Mapping methane emissions from a marine geological seep source using imaging spectrometry, *Remote Sens. Environ.*, *114*(3), 592–606, doi:10.1016/j.rse.2009.10.015.

Schneising, O., et al. (2009), Three years of greenhouse gas column-averaged dry air mole fractions retrieved from satellite—Part 2: Methane, *Atmos. Chem. Phys.*, *9*(2), 443–465, doi:10.5194/acp-9-443-2009.

Yoshida, Y., et al. (2010), Retrieval algorithm for $CO_2$ and $CH_4$ column abundances from short-wavelength infrared spectral observations by the Greenhouse Gases Observing Satellite, *Atmos. Meas. Tech. Discuss.*, *3*(6), 4791–4833, doi:10.5194/amtd-3-4791-2010.

E. S. Bradley, D. A. Roberts, and L. Washburn, Department of Geography, University of California, Santa Barbara, CA 93106, USA. (ebradley@geog.ucsb.edu)

P. E. Dennison, Department of Geography, University of Utah, Salt Lake City, UT 84112, USA.

I. Leifer, Marine Science Institute, University of California, Santa Barbara, CA 93106, USA.